IMPROVED BOUNDARY-INTEGRAL EQUATION METHOD FOR TIME-DEPENDENT INELASTIC DEFORMATION IN METALS

MAHESH MORJARIA
AND
SUBRATA MUKHERJEE

DEPARTMENT OF THEORETICAL AND
APPLIED MECHANICS
CORNELL UNIVERSITY
ITHACA, NY 14853

DOE Report No. COO-2733-20

Prepared by Cornell University
under Department of Energy
Contract No. EG-77-S-02-2733

February 1979

DISCLAIMER

SUMMARY

Efficient solution of boundary-value problems for time-dependent inelastic deformation in metallic structures is of great practical importance. These problems are generally solved by finite element methods and separate descriptions for time-independent plasticity and time-dependent creep are normally used. The boundary-integral equation method was recently applied for the first time to such problems. This paper presents a very efficient numerical implementation of the method with a linear description of the relevant variables over each boundary element and a newly developed Euler type time-integration scheme with automatic time-step control for time integration. Numerical results for plates in plane stress with and without cutouts, under different loading histories, are presented. A combined creep-plasticity constitutive theory with state variables is used to model material behavior. The results are more accurate and are obtained with much less computational effort compared to a previous attempt with an uniform description of variables over each boundary element and a predictor-corrector scheme for time-integration. The computer program developed is quite general and can handle plane stress problems for plates of arbitrary shapes subjected to arbitrary time-histories of loadings. The numerical results presented in the paper are for certain illustrative problems.

INTRODUCTION

The boundary-integral equation (BIE) method has been applied to various problems in solid mechanics by many authors. Recently, it has been used to solve boundary value problems in time-independent plasticity[1-4] and time-dependent inelastic deformation[5-6]. Boundary value problems involving time-dependent inelastic deformation are particularly challenging since the process is nonlinear and time and history dependent. Finite element methods (FEM) are mostly being used for such problems and the calculations are generally quite expensive[7]. The BIE method is being explored as a possible alternative to FEM for this class of problems and particular attention is being paid to the accuracy and efficiency of this approach.

Mukherjee and Kumar[5-6] recently used the BIE method to solve two-dimensional inelasticity problems. A rate formulation of the governing differential equations was used, with the spatial equations being solved at each time by the BIE method, coupled with a scheme for integrating in time. Material behavior was described either by the equations of power law creep[8] or the state variable model due to Hart[9-10]. Hart's is one of several state variable constitutive models of inelastic deformation (eg.[9-15]) that have been proposed recently. Many of these state variable models have a mathematical structure that is particularly suitable for the rate formulation in that the nonelastic strain rate at any time is a function of stress and state variables but not the rates of stress or displacement. Hart's model has been shown to faithfully reproduce experimentally observed material behavior in a variety of cases[16] and is used in the numerical calculations presented later in the paper.

The computer program used to obtain the numerical results reported in[6] contained a spatially uniform description of the relevant variables over each boundary element and a predictor-corrector scheme for time-integration. While the paper demonstrated the feasibility of the BIE method for this class of problems, several shortcomings remained with regard to solution efficiency and the range of problems that could be solved. A tremendous improvement in the accuracy and efficiency of the computer program has been achieved by making two important modifications. The first is the use of a spatially linear distribution of traction and displacement on each boundary element. This markedly improves the representation of the variables on the boundary, thus greatly improving accuracy for the same number of boundary elements. The second is the incorporation of a recently developed Euler-type time integration scheme with automatic time-step control which speeds up the time-integration process without sacrificing accuracy[17]. These modifications make it possible to solve problems of practical interest (eg. a plate in creep in plane stress with an elliptical cutout under uniaxial tension) that could not be solved before and reduce computer times by almost an order of magnitude in some cases. There is no loss of accuracy when using the current version of the program. Comparisons of the two versions of the program are presented in a table later in the paper.

A brief review of the state variable models of inelastic deformation with particular reference to Hart's model is followed by the BIE formulation with linearly varying boundary tractions and displacements. Numerical implementation of the equations is discussed next, followed by numerical results for various cases. Some of these results are compared with those obtained by direct means and the computations are examined with regard to accuracy and efficiency.

MATHEMATICAL STRUCTURE OF STATE VARIABLE MODELS

The mathematical structure of many of the state variable models of inelastic deformation can be summarised by the following equations

$$\dot{\varepsilon}_{ij} = \dot{\varepsilon}^{e}_{ij} + \dot{\varepsilon}^{n}_{ij} + \dot{\varepsilon}^{T}_{ij} \tag{1}$$

$$\dot{\varepsilon}^{n}_{ij} = f_{ij}(\sigma_{ij}, q^{(k)}_{ij}, T) \tag{2}$$

$$\dot{q}^{(k)}_{ij} = g_{ij}(\sigma_{ij}, q^{(k)}_{ij}, T) \tag{3}$$

$$\dot{\varepsilon}^{n}_{kk} = 0 \tag{4}$$

Here $\dot{\varepsilon}^{e}_{ij}$, $\dot{\varepsilon}^{n}_{ij}$ and $\dot{\varepsilon}^{T}_{ij}$ are the elstic, nonelastic and thermal strain rates respectively, σ_{ij} is the stress tensor, T the temperature and $q^{(k)}_{ij}$ are state variables. The number of state variables vary in the different models and they can be scalars or tensors. These state variables are assumed to completely characterize the present deformation state of the material and the history dependence of the rate of nonelastic strain upto the current time is assumed to be completely taken into account by their current values. It is important to note that the rates of the nonelastic strain and state variables at any time depend only on the current values of the stress, state variables and temperature. This fact plays a key role in the BIE formulation presented in the next section.

The specific equations for Hart's constitutive model are presented next. According to this model, the nonelastic strain is decomposed into two (time-dependent) components

$$\dot{\varepsilon}^{n}_{ij} = \dot{\varepsilon}^{a}_{ij} + \dot{\varepsilon}^{p}_{ij} \tag{5}$$

where ε^a_{ij} is the anelastic strain, a stored strain which reflects the magnitude and direction of prior deformation history and ε^p_{ij} is the completely irrecoverable and path dependent permanent strain. The two state variables in the model are the anelastic strain and a scalar σ^*, called hardness, which is similar to an isotropic strain hardening parameter.

Let s_{ij} represent the deviatoric part of the stress tensor σ_{ij}. The deviatoric stress tensor is decomposed into two auxilliary tensors s^a_{ij} and s^f_{ij}

$$s_{ij} = s^a_{ij} + s^f_{ij} \tag{6}$$

The flow relations for the anelastic strain and the time rates of change of the permanent and nonelastic strains are

$$\varepsilon^a_{ij} = \frac{3}{2}\frac{\varepsilon^a}{\sigma^a}s^a_{ij} \qquad \dot{\varepsilon}^p_{ij} = \frac{3}{2}\frac{\dot{\varepsilon}^p}{\sigma^a}s^a_{ij} \tag{7,8}$$

$$\dot{\varepsilon}^n_{ij} = \frac{3}{2}\frac{\dot{\varepsilon}^n}{\sigma^f}s^f_{ij} \tag{9}$$

where $\dot{\varepsilon}^n$, $\dot{\varepsilon}^p$, ε^a, σ, σ^a and σ^f are scalars defined as

$$\dot{\varepsilon}^n = \sqrt{(\tfrac{2}{3}\,\dot{\varepsilon}^n_{ij}\dot{\varepsilon}^n_{ij})}\ , \quad \dot{\varepsilon}^p = \sqrt{(\tfrac{2}{3}\,\dot{\varepsilon}^p_{ij}\dot{\varepsilon}^p_{ij})}\ , \quad \varepsilon^a = \sqrt{(\tfrac{2}{3}\,\varepsilon^a_{ij}\varepsilon^a_{ij})} \tag{10}$$

$$\sigma = \sqrt{(\tfrac{3}{2}\,s_{ij}s_{ij})}\ , \quad \sigma^a = \sqrt{(\tfrac{3}{2}\,s^a_{ij}s^a_{ij})}\ , \quad \sigma^f = \sqrt{(\tfrac{3}{2}\,s^f_{ij}s^f_{ij})}\ .$$

The scalar invariants are related to each other through the uniaxial equations

$$\sigma^a = M\varepsilon^a \quad , \qquad \dot{\varepsilon}^n = \dot{a}^*(\sigma^f/M)^M \tag{11,12}$$

$$\dot{\varepsilon}^{p} = \dot{\varepsilon}^{*}(\ell n(\sigma^{*}/\sigma^{a}))^{-1/\lambda} \tag{13}$$

$$\dot{\varepsilon}^{*} = \varepsilon^{*}_{sT}(\sigma^{*}/\sigma^{*}_{s})^{m}\exp(Q/RT_{B})\exp(-Q/RT) \tag{14}$$

$$\dot{\sigma}^{*} = \dot{\varepsilon}^{p}\sigma^{*}\Gamma(\sigma^{*},\sigma^{a}) \quad , \qquad \Gamma(\dot{\sigma}^{*};\sigma^{a}) = (\beta/\sigma^{*})^{\delta}(\sigma^{a}/\sigma^{*})^{\beta/\sigma^{*}} \tag{15,16}$$

Equation (11) represents a linear anelastic element, (12) a nonlinear dashpot, (13) and (14) a "plastic" element and, finally, (15) and (16) describe strain hardening. The flow parameters are $\mathcal{M}$, M, m, λ, a^{*} and $\dot{\varepsilon}^{*}_{sT}$ (at a reference hardness level σ^{*}_{s} and reference temperature T_{B}); β and δ are strain hardening parameters, R is the gas constant and Q the activation energy for atomic self diffusion. The material parameters, many of which are temperature dependent, are obtained from load relaxation and constant strain rate tension experiments. They are given in Appendix A of the EPRI report by Kumar and others[16].

IMPROVED BOUNDARY-INTEGRAL EQUATION METHOD FOR TIME-DEPENDENT INELASTIC DEFORMATION IN METALS

MAHESH MORJARIA
AND
SUBRATA MUKHERJEE

DEPARTMENT OF THEORETICAL AND
APPLIED MECHANICS
CORNELL UNIVERSITY
ITHACA, NY 14853

DOE Report No. COO-2733-20

Prepared by Cornell University
under Department of Energy
Contract No. EG-77-S-02-2733

February 1979

BOUNDARY-INTEGRAL EQUATION FORMULATION AND SOLUTION STRATEGY

The boundary integral equations for planar problems and the strategy for obtaining solutions to these time-dependent problems are presented in this section. The range of subscript indices in all the equations in this section is 1, 2.

BIE formulation for plane stress

The Navier equations for displacement rates for plane stress in the presence of nonelastic strain rates are[5-6]

$$\dot{u}_{i,kk} + \frac{1+\nu}{1-\nu}\dot{u}_{k,ki} = -\frac{\dot{F}_i}{G} + 2\dot{\varepsilon}^n_{ij,j} + \frac{2\nu}{1-\nu}\dot{\varepsilon}^n_{kk,i} + \frac{2(1+\nu)}{1-\nu}(\alpha\dot{T})_{,i} \qquad (17)$$

where F_i is the prescribed body force/unit volume, G and ν are the shear Modulus and Poisson's ratio, α is the coefficient of linear thermal expansion and u_i is the displacement vector. Suitable traction and displacement rate boundary conditions must be prescribed. An integral representation of the solution can be obtained using Kelvin's singular solution for the corresponding elastic problem. This is[5-6]

$$\dot{u}_i(p) = \int_S [U_{ij}(P,Q)\dot{\tau}_j(Q) - T_{ij}(P,Q)\dot{u}_j(Q)]dS_Q$$

$$+\int_V U_{ij}(p,q)\dot{F}_j(q)dV_q$$

$$+\int_V \Sigma_{jki}(p,q)[\dot{\varepsilon}^n_{jk}(q) + \delta_{jk}\alpha\dot{T}(q)]dV_q \qquad (18)$$

where P and Q are surface points, p and q are interior points and V is the volume and S the surface of the body. The kernels U_{ij}, T_{ij} and Σ_{jki} are known singular solutions due to a point load in an infinite elastic solid in plane stress and are available in many references (eg. [2,5,18]).

All the traction and displacement components in equation (18), are, of course, not known a priori over the entire surface S. A system of integral equations for the unspecified components of boundary traction and displacement rates is obtained by taking the limit as p in V approaches an arbitrary point P on S. The resulting equation for the plane stress case, when P lies on a boundary corner of included angle β [Figure 1] is[4]

$$(\delta_{ij}-c_{ij})\dot{u}_j(P) = \int_S [U_{ij}(P,Q)\dot{\tau}_j(Q)-T_{ij}(P,Q)\dot{u}_j(Q)]dS_Q + \int_V U_{ij}(P,q)\dot{F}_j(q)dV_q + \int_V \Sigma_{jki}(P,q)[\dot{\varepsilon}^n_{jk}(q)+\delta_{jk}\alpha\dot{T}(q)]dV_q \tag{19}$$

where
$$c_{11} = 1-\frac{\beta}{2\pi}-\frac{\cos(2\gamma)\sin\beta}{4\pi(1-\nu)}$$
$$c_{12} = c_{21} = -\frac{\sin(2\gamma)\sin\beta}{4\pi(1-\nu)}$$
$$c_{22} = 1-\frac{\beta}{2\pi}+\frac{\cos(2\gamma)\sin\beta}{4\pi(1-\nu)} \tag{20}$$

where δ_{ij} is the Kronecker delta and γ is the angle between the bisector of β and the x_1 axis. If the boundary at P is locally smooth, $\beta = \pi$ and $c_{11} = c_{22} = 1/2$, $c_{12} = 0$. Consideration of approaching a corner on the boundary is necessary since in the linear formulation values of tractions and displacements are assigned at the boundary nodes located at the intersections of segments, rather than at the centroids of these segments. Each segment is assumed straight.

Finally, the stress rates are obtained from the elastic strain rates by using Hooke's law. This equation has the following form for plane stress

$$\dot{\sigma}_{ij} = G\Big[(\dot{u}_{i,j}+\dot{u}_{j,i}) + \frac{2\nu}{1-\nu}\,\dot{u}_{k,k}\delta_{ij} - 2\dot{\varepsilon}^{n}_{ij} - \left(\frac{2\nu}{1-\nu}\right)\dot{\varepsilon}^{n}_{kk}\delta_{ij} - \frac{2(1+\nu)}{1-\nu}\,\alpha\dot{T}\delta_{ij}\Big] \qquad (21)$$

Equation (21) is used in a different form in the numerical implementation in order to avoid numerical differentiation.

The formulation for plane strain is analogous to that for plane stress[2,5,18].

Solution strategy

The initial distribution of state variables is prescribed and the initial nonelastic strain is set to be zero. The initial distribution of stresses and displacements is obtained from the solution of the corresponding thermo-elastic problem. The rate of the nonelastic strain at $t = 0$ is obtained from equation (2) (the temperature and body force fields are assumed to be known for all time). These nonelastic strain rates are used in equation (19), which is solved to obtain the unspecified components of boundary traction and displacement rates at $t = 0$. The displacement and stress rates throughout the body are now obtained from equations (18) and (21) and the rates of change of the state variables from equation (3). The values of these quantities at a new time Δt are now obtained by integrating forward in time using a suitable numerical procedure. Since the state variable equations are generally stiff, choice of a suitable time-integration scheme is crucial. An Euler type strategy with automatic time-step control is used[17]. A brief discussion of this method is presented in the next section.

NUMERICAL IMPLEMENTATION

Numerical implementation of the boundary integral equations and the time-integration strategy are discussed in this section.

Numerical implementation of BIE

The boundary of the planar body, S, is divided into N_s straight boundary elements and the interior into n_i polygonal internal elements. The components of traction and displacement and their rates are assumed to vary linearly over each boundary segment, with their values assigned at the nodes which lie at the intersection of the segments. The components of stress and state variables are assumed to be spatially uniform over an internal element. This formulation guarantees continuity of displacement across each boundary node since two adjacent segments share the same node. The tractions, however, must be allowed to have discontinuities across a node whenever necessary. This is taken care of by placing a "zero length" element between two nodes, and assigning different traction values at each of these nodes. The contributions of zero length segments to integrals associated with such segments have been shown to vanish[4].

A discrete analog of the boundary integral equation (19) (with $\dot{F}_j = \dot{T} = 0$) can be written as

$$
\begin{aligned}
(\delta_{ij}-c_{ij})\dot{u}_j(P_M) &= \sum_{N_S} \int_{\Delta S_N} U_{ij}(P_M,Q)\dot{\tau}_j(Q)\,dS_Q \\
&- \sum_{N_S} \int_{\Delta S_N} T_{ij}(P_M,Q)\dot{u}_j(Q)\,dS_Q \\
&+ \sum_{n_i} \dot{\varepsilon}^n_{jk}(q_n)\Delta\Sigma_{jki}(P_M,q_n)
\end{aligned}
$$

$$(i,j,k = 1,2, \quad M = 1,2,\ldots \dot{N}_S) \qquad (21)$$

where $\Delta\Sigma_{jki}(P_M,q_n) = \int_{\Delta V_n} \Sigma_{jki}(P_M,q)dV_q$

and $u_j(P_M)$ are displacement components at a point P which coincides with node M. The nonelastic strain rate is assumed to be uniform over an internal element and is therfore factored out of the integral sign, but the displacement and traction rates are nonuniform and remain inside the integral signs at this stage.

The linear variation of displacement and traction rates within the N_{th}, segment is represented as

$$\dot{u}_i(Q) = \frac{(\dot{u}_i(Q_{N_b})-\dot{u}_i(Q_{N_a}))}{\Delta S_N} s + \dot{u}_i(Q_{N_a})$$

$$\dot{\tau}_i(Q) = \frac{(\dot{\tau}_i(Q_{N_b})-\dot{\tau}_i(Q_{N_a}))}{\Delta S_N} s + \dot{\tau}_i(Q_{N_a}) \qquad (22)$$

where N_a and N_b are two nodes on either side of segment N as shown in Figure 1 and S is the distance measured from N_a. Substitution of equations (22) into (21) leads to a matrix equation of the type

$$[A]\{\dot{u}\} = [B]\{\dot{\tau}\} + \{\dot{b}\} \qquad (23)$$

where the coefficient matrices $\underline{A}$ and $\underline{B}$ contain integrals of the type

$$\int_{\Delta S_N} U_{ij}(P_M,Q)dS_Q \; , \quad \int_{\Delta S_N} U_{ij}(P_M,Q)\, s dS_Q$$

and the vector $\underline{b}$ involves $\Delta\Sigma_{jki}$ and the nonelastic strain rates. Integrals involving these kernels have been evaluated in closed form for straight boundary elements and polygonal internal elements. Details of these calculations are available in the ERDA report[19] and Riccardella[4].

Equations (23) are solved for the unknown components of traction and displacement rates. Once all these are known, they are used in a discrete analog of equation (18) to obtain the displacement rates throughout the body. In contrast to finite element methods, the number of unknowns in equation (23) are governed by the number of boundary elements only and the interior values are obtained by multiplying known matrices and vectors.

The stress rates inside the body are finally obtained from the displacement rates in a manner described in an earlier paper by Mukherjee and Kumar[6].

Time Integration

As mentioned earlier, many of the state variable constitutive models give rise to stiff systems of differential equations and it is very important that a suitable time integration strategy with automatic time step control be used. An Euler type strategy which is simple yet very efficient is used to obtain the numerical results discussed later in the paper. A brief summary of the method in terms of a single differential equation

$$\frac{dy}{dt} = F(y,t) \tag{24}$$

is presented below. Further details are available in Kumar et al[17]. The value of $y(t+\Delta t)$ in terms of $y(t)$ is

$$y(t+\Delta t) = y(t) + F(y,t)\Delta t \tag{25}$$

and the error at this step used for automatic time step control is defined as

$$e = \Delta t|\nabla F|/|y(t)| \tag{26}$$

where $\nabla F = F(y,t)-F(y,t-\Delta t_{previous})$, is the first backward difference of F. Two error parameters e_{max} and e_{min} are initially prescribed. The algorithm proceeds as follows:

$$e_{max} < e: \quad \text{replace } \Delta t \text{ by } \Delta t/2\text{; recompute } e.$$

$$e \leq e_{max}: \quad \text{accept } \Delta t\text{; calculate } y(t+\Delta t)$$

The time step for the next step, Δt_{next}, is decided according as

$$e_{min} < e \leq e_{max}: \quad \Delta t_{next} = \Delta t$$

$$e \leq e_{min} \quad : \quad \Delta t_{next} = 2\Delta t$$

The problem at hand, of course, involves systems of such equations for the rates of variables at the boundary and internal nodes. In this case the error e_i for the i_{th} variable is defined as an L^1 norm of the type

$$e_i = \frac{\Delta t \, \Sigma \, |\nabla F_k|}{\Sigma \, |y_k(t)|} \tag{27}$$

where the summation extends over the values of the i_{th} variable over all the nodes; and then

$$e = \max|e_i| \tag{28}$$

The algorithm then proceeds as described above.

NUMBERICAL RESULTS AND DISCUSSION

Numerical results for various cases for 304 stainless steel plates in plane stress at 200°C and 400°C, using Hart's constitutive model, are presented in Figures 2-7. Figures 2-5 present comparisons with results obtained by direct means and Figures 6-7 present results for a plate with an elliptic cutout. In all cases, only a quarter of the plate is modelled because of symmetry. Boundary and internal elements are distributed uniformly over uniform square plates (Figures 2-3) and the mesh distributions used in the other cases are given in Figures 4 and 6. The square plates (Figures 2-3, 6-7) are of side 2 in. and the circular plate with concentric circular cutout (Figures 4-5) has a ratio of outside to inside radius equal to 1.5.

<u>Parameter values</u>

The values of various parameters at 400°C[16] are given below and those at 200°C are available in Kumar et al[16].

$$\lambda = 0.15 \qquad M = 7.8 \qquad m = 5$$

$$\mathcal{M} = 0.132 \times 10^{8} \text{ psi} \qquad E = 0.244 \times 10^{8} \text{ psi}$$

$$\nu = 0.298$$

$$\dot{a}^* = 0.69 \times 10^{25} \text{ sec}^{-1}$$

$$\dot{\varepsilon}^*_{sT} = 1.269 \times 10^{-24} \quad \text{at} \quad \sigma^*_s = 10 \text{ ksi}, \quad T_B = 400°\text{C}$$

$$\beta = 0.179 \times 10^{6} \text{ psi} \qquad \delta = 1.33$$

The initial values of the state variables are

$$\sigma^*(\underline{x},0) = 17 \text{ ksi} \quad , \qquad \varepsilon^a_{ij}(\underset{\sim}{x},0) = 0 \quad .$$

Comparisons with direct calculations

Results obtained by the BIE method for one dimensional creep and tension tests are compared with those from direct numerical integration[16] in Figures 2-3. The comparisons with just 4 boundary elements and one internal element are excellent. The tension test results are much more accurate than the previous attempt[6] with spatially uniform variables over each boundary element, although only 4 instead of 20 boundary elements are used. The creep problem could not be solved by the previous version of the program since comulative numerical errors gave rise to unacceptably large (instead of zero) transverse stresses after some hours of simulated time.

Results for a circular disc with circular cutout, under internal pressure increasing at a constant rate, are shown in Figure 5. The boundary and internal mesh for this problem are shown in Figure 4. The direct solution for this problem is discussed in Mukherjee[20]. Again, the comparison is very good for this problem which involves redistribution of radial and tangential stresses.

Square plates with cutouts

Inelastic deformation of a square plate with a circular cutout was analysed with the same mesh as before[6] and the results compared very well with earlier results[6].

Results for a square plate with an elliptic cutout are shown in Figure 7 with the corresponding boundary and internal mesh shown in Figures 6(a)-6(c). The ratio of axes of the ellipse is 4 and this leads to an elastic stress concentration factor of about 10 at the point A in Figure 6(a). Thus, there is a severe spatial stress gradient initially and plastic flow causes very rapid relaxation of stresses near the cutout. Redistribution of stress with time on the line AJ (Figure 6(a)) is shown in Figure 7. Large stress gradients in time are seen to exist. The elastic solution is within about 4% of the correct solution near the cutout and more accurate away from it. This problem could not be solved in the previous attempt[6].

Comparison of computing times for previous and present cases

The CPU times on an IBM 370/168 and number of elements for these problems, together with comparisons with the previous attempt[6] whenever available, are shown in Table 1. It is seen that savings in computer time are of an order of magnitude and problems which could not be solved in the previous attempt can now be solved efficiently due to great improvement in accuracy. The computer time for the plate with elliptic cutout for a simulation time of 100 hours of creep is only 152 seconds. The present version of the program, with linear variation of variables over the boundary elements and the Euler type time-integration scheme with automatic time-step control, seems very efficient.

CONCLUSIONS

Efficient solution of nonlinear time-dependent inelasticity problems with material behavior modelled by realistic constitutive relations is both challenging and important from the viewpoint of design. It appears from the results in this paper that the BIE method is a powerful computational procedure for the efficient solution of such problems.

ACKNOWLEDGEMENTS

This research was supported by Contract No. EG-77-S-02-2733 of the U.S. Department of Energy with Cornell University.

REFERENCES

1. J.L. Swedlow and T.A. Cruse, 'Formulation of boundary-integral equations for three-dimensional elasto-plastic flow', Int. J. Solids Struct. 7, 1673-1683 (1971).

2. A. Mendelson, 'Boundary integral methods in elasticity and plasticity', Report No. NASA TND-7418 (1973).

3. A. Mendelson and L.U. Albers, 'Application of boundary-integral equations to elastoplastic problems', Boundary-Integral Equation Method: Computational Applications in Applied Mechanics, T.A. Cruse and F.J. Rizzo eds., ASME, 47-84 (1975).

4. P.C. Riccardella, 'An implementation of the boundary-integral technique for planar problems in elasticity and elasto-plasticity', Report No. SM-73-10, Department of Mechanical Engineering, Carnegie-Mellon University, Pittsburg (1973).

5. V. Kumar and S. Mukherjee, 'A boundary-integral equation formulation for time-dependent inelastic deformation in metals', Int. J. Mech. Sci. 19, 713-724 (1977).

6. S. Mukherjee and V. Kumar, 'Numerical analysis of time-dependent inelastic deformation in metallic media using the boundary-integral equation method', ASME J. Appl. Mech. 45, 785-790 (1978).

7. Y.S. Pan and H.M. Minami, 'Inelastic analysis of nozzle-to-spherical shell attachemnt', Inelastic Behavior of Pressure Vessel and Piping Components, T.Y. Cahng and E. Krempl eds., ASME, 103-120 (1978).

8. R.K. Penney and D.L. Marriott, Design for Creep, McGraw Hill, London, 1971.

9. E.W. Hart, C.Y. Li and H. Yamada, 'Phenomenological theory - a guide to constitutive relations and fundamental deformation properties', Constitutive Equations in Plasticity, A.S. Argon ed., MIT Press, Cambridge, Mass., 149-197 (1976).

10. E.W. Hart, 'Constitutive relations for the nonelastic deformation of metals', ASME J. Engng. Mat. Tech., 98, 193-202 (1976).

11. A. Miller, 'An inelastic constitutive model for monotonic, cyclic and creep deformation: Part 1 - Equations developement and analytical procedures', ASME J. Engng. Mat. Tech., 98, 97-105 (1976).

12. A. Miller, 'An inelastic constitutive model for monotonic, cyclic and creep deformation: Part 2 - Application to type 304 stainless steel', ASME J. Engng. Mat. Tech., 98, 106-113 (1976).

13. E.P. Cernocky and E. Krempl, 'Viscoplasticity based on total strain', Abstracts of the Eighth U.S. National Congress of Applied Mechanics, UCLA, Los Angeles (1978).

14. R.D. Krieg, 'A physically based internal variable model for rate-dependent plasticity', Inelastic Behavior of Pressure Vessel and Piping Components, T.Y. Chang and E. Krempl eds., ASME, 15-28 (1978).

15. A.R.S. Ponter and F.A. Leckie, 'Constitutive relationships for the time-dependent deformation of metals; ASME J. Engng. Mat. Tech., 98, 47-51 (1976).

16. V. Kumar, F. Huang, S. Mukherjee and C.Y. Li, 'Theoretical and experimental analysis of stresses in reactor components - Deformation in type 304 stainless steel', EPRI final report for Contract No. RP 697-1, Department of Materials Science and Engineering, Cornell University, Ithaca, NY (1979).

17. V. Kumar, M. Morjaria and S. Mukherjee, 'Numerical integration of some stiff constitutive models of inelastic deformation', ASME J. Engng. Mat. Tech. In press.

18. S. Mukherjee, 'Corrected boundary-integral equations in planar thermo-elastoplasticity', Int. J. Solids Struct. 13, 331-336 (1977).

19. S. Mukherjee and V. Kumar, 'Numerical analysis of time-dependent inelastic deformation in metallic media using the boundary-integral equation method', ERDA Report No. COO-2733-14, Department of Theoretical and Applied Mechanics, Cornell University, Ithaca, NY (1977).

20. S. Mukherjee, 'Thermoviscoelastic response of cylindrical structures using a state variable theory', Proceedings of the 3rd International Conference on Mechanical Behavior of Materials, Cambridge, England (1979). In press.

Problem	Number of Boundary Elements		Number of Internal Elements		CPU time(sec) IBM 370/168	
	Reference 6	Present	Reference 6	Present	Reference 6	Present
1. Uniaxial Creep (Figure 2)		4		1		7.3
2. Uniaxial extension (Figure 3)	20	4	1	1	150	3.9
3. Circular plate under increasing internal pressure (Figures 4-5)		30		20		63
4. Square plate with circular cutout under constant remote tension (304 SS, 400°C, σ_{22}^{∞} = 10 ksi)	38	37	20	20	600	91
5. Square plate with elliptic cutout under constant remote tension (Figures 6-7)		38		30		152

Table 1. Program Statistics and Comparison with reference 6.

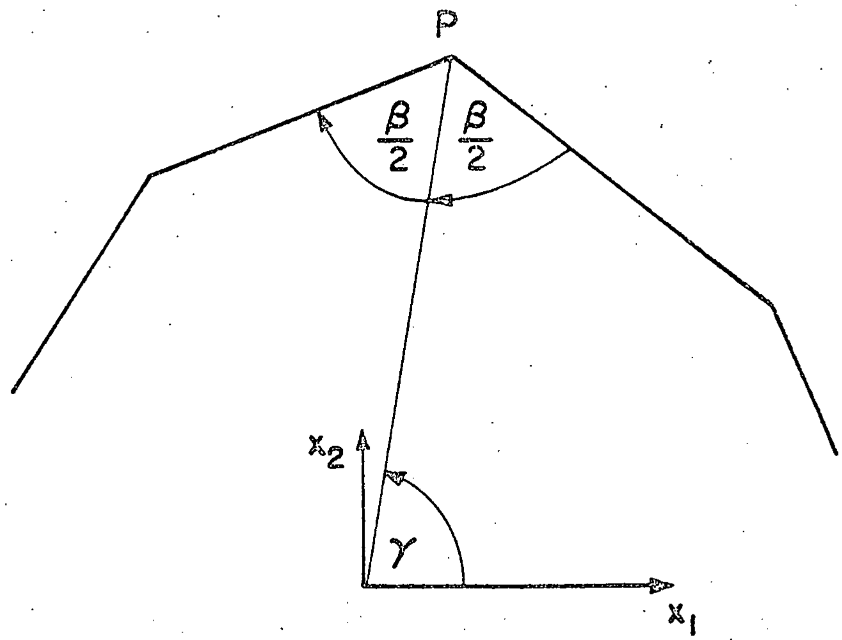

(a)

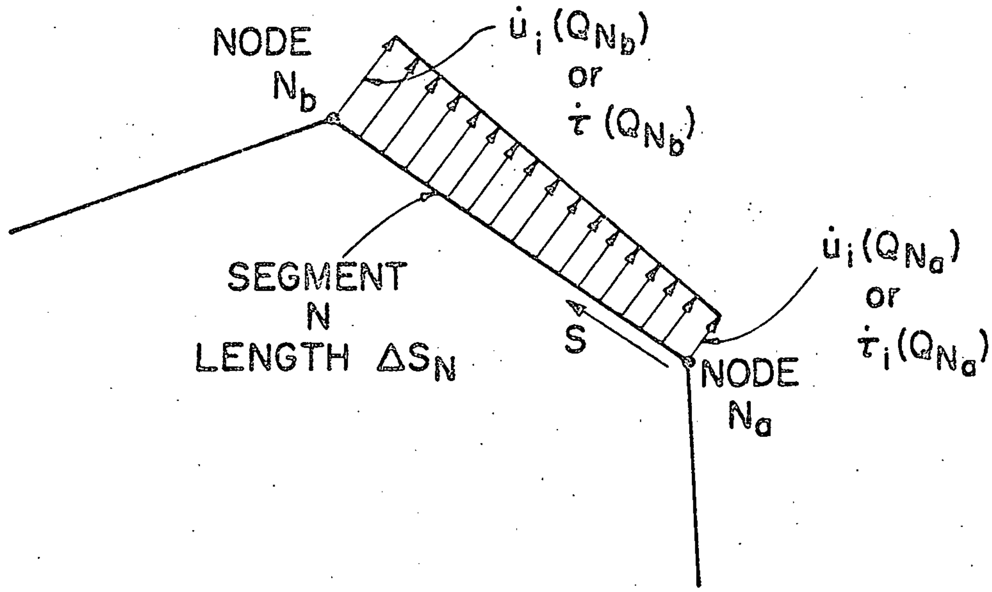

(b)

Figure 1. (a) Limiting procedure for internal point approaching a boundary corner.
(b) Linear representation of variables on a boundary segment.

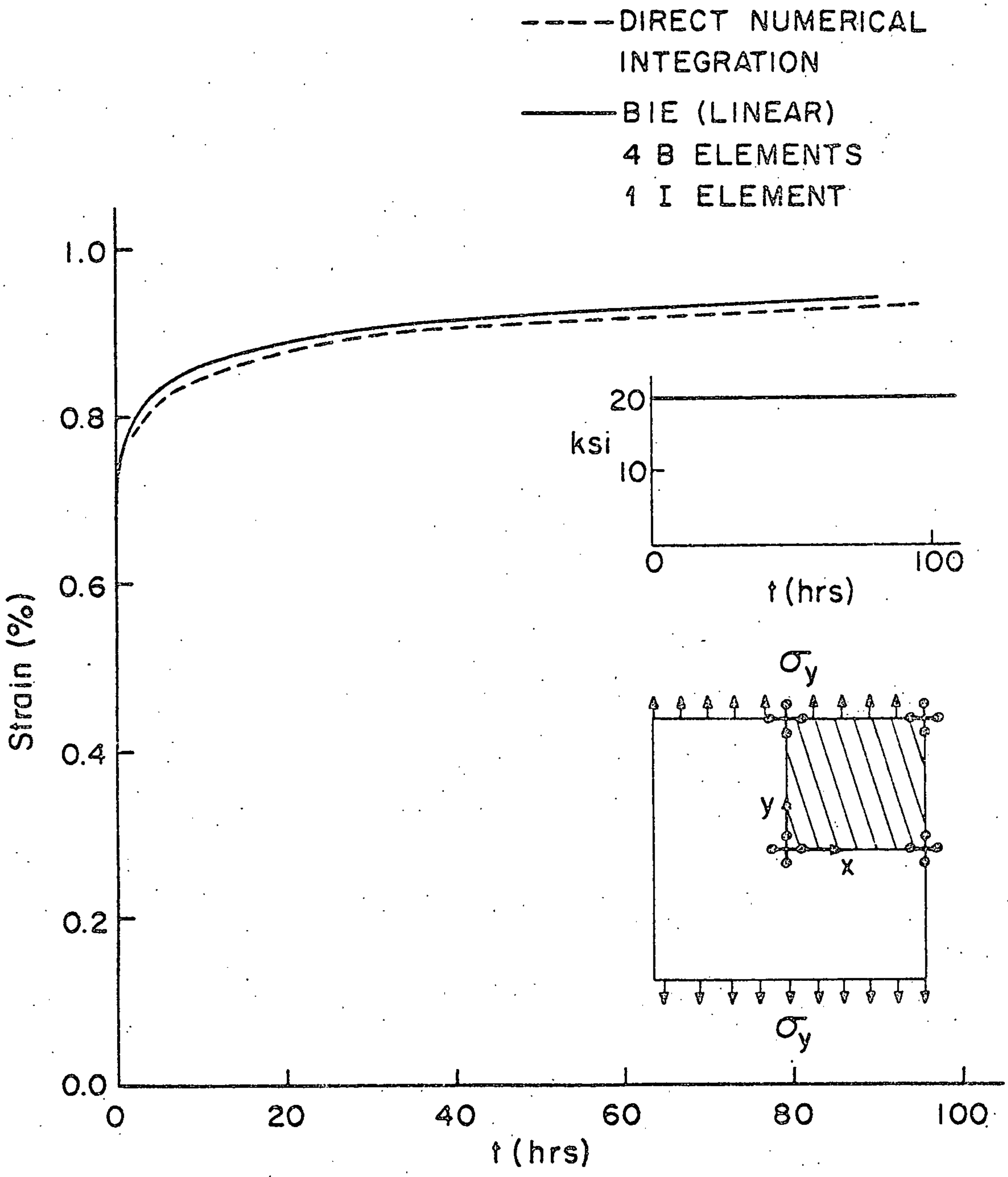

Figure 2. Comparison of direct and BIE solutions for uniaxial creep at a constant stress of 20 ksi in an annealed 304 SS plate at 400°C.

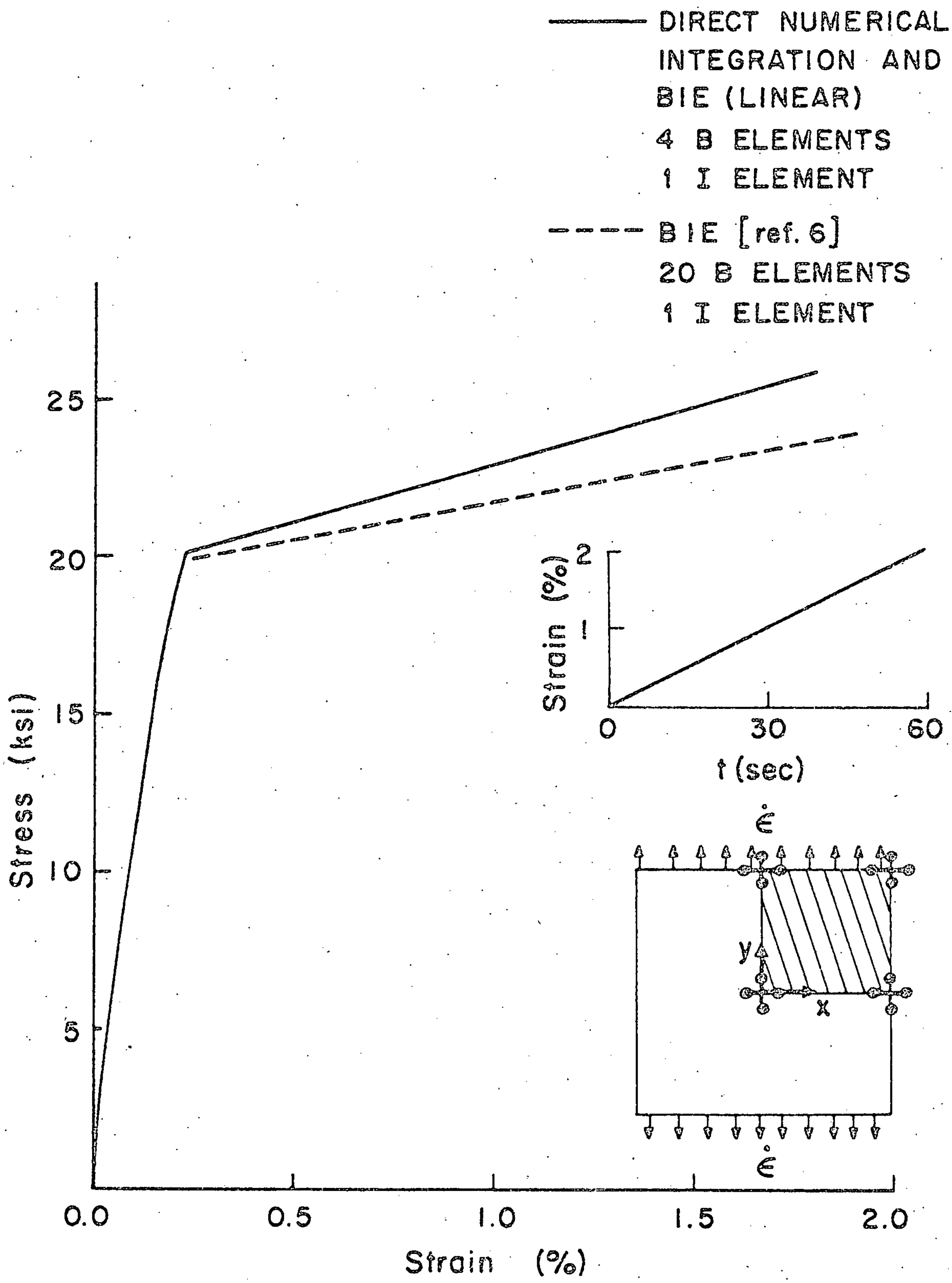

Figure 3. Comparison of direct, BIE (linear) and BIE (constant) solutions for applied displacement increasing at a constant rate in an annealed 304 SS plate at 400°C.

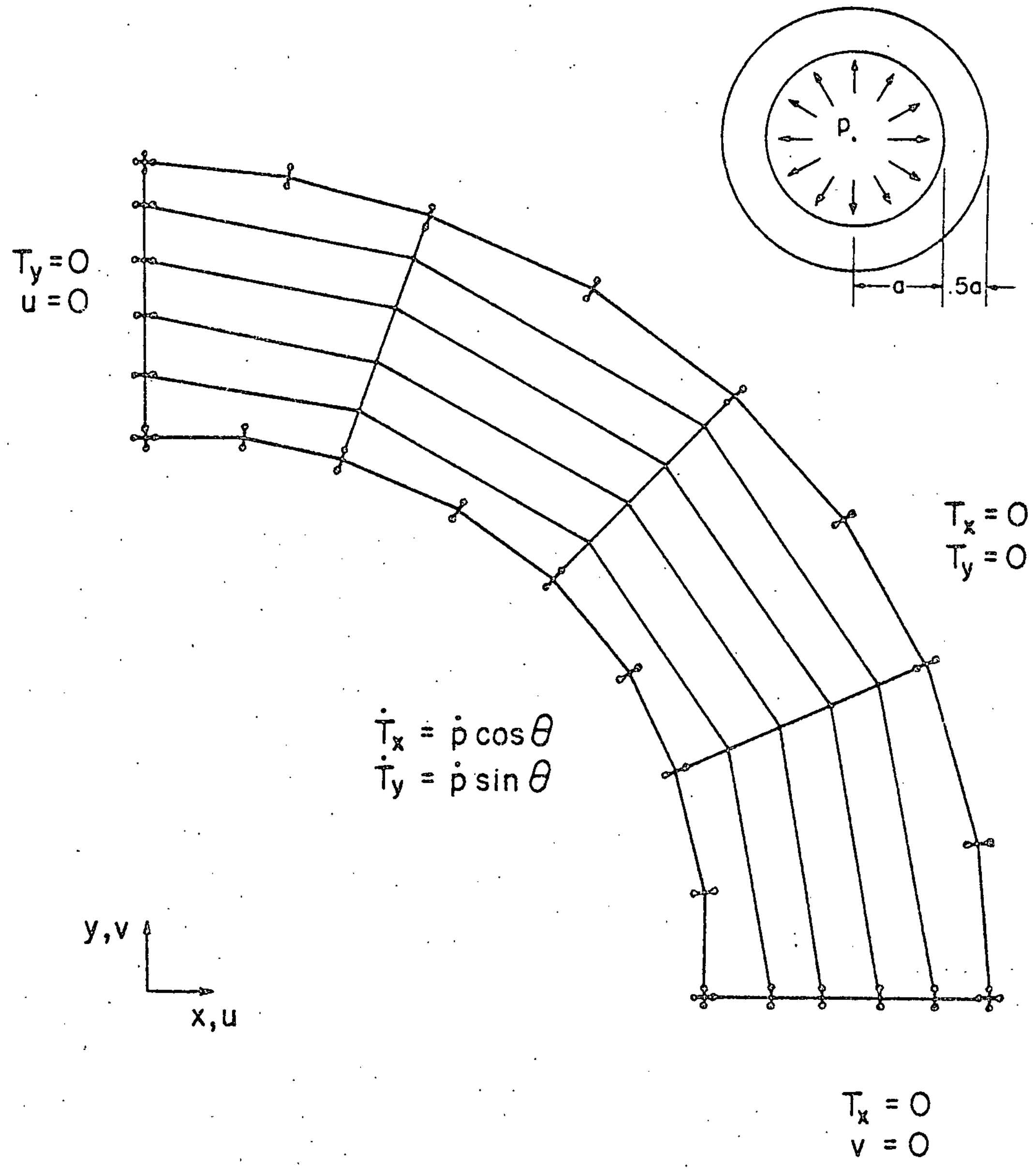

Figure 4. Boundary and internal elements for circular plate with concentric circular cutout under internal pressure. 30 boundary elements and 20 internal elements.

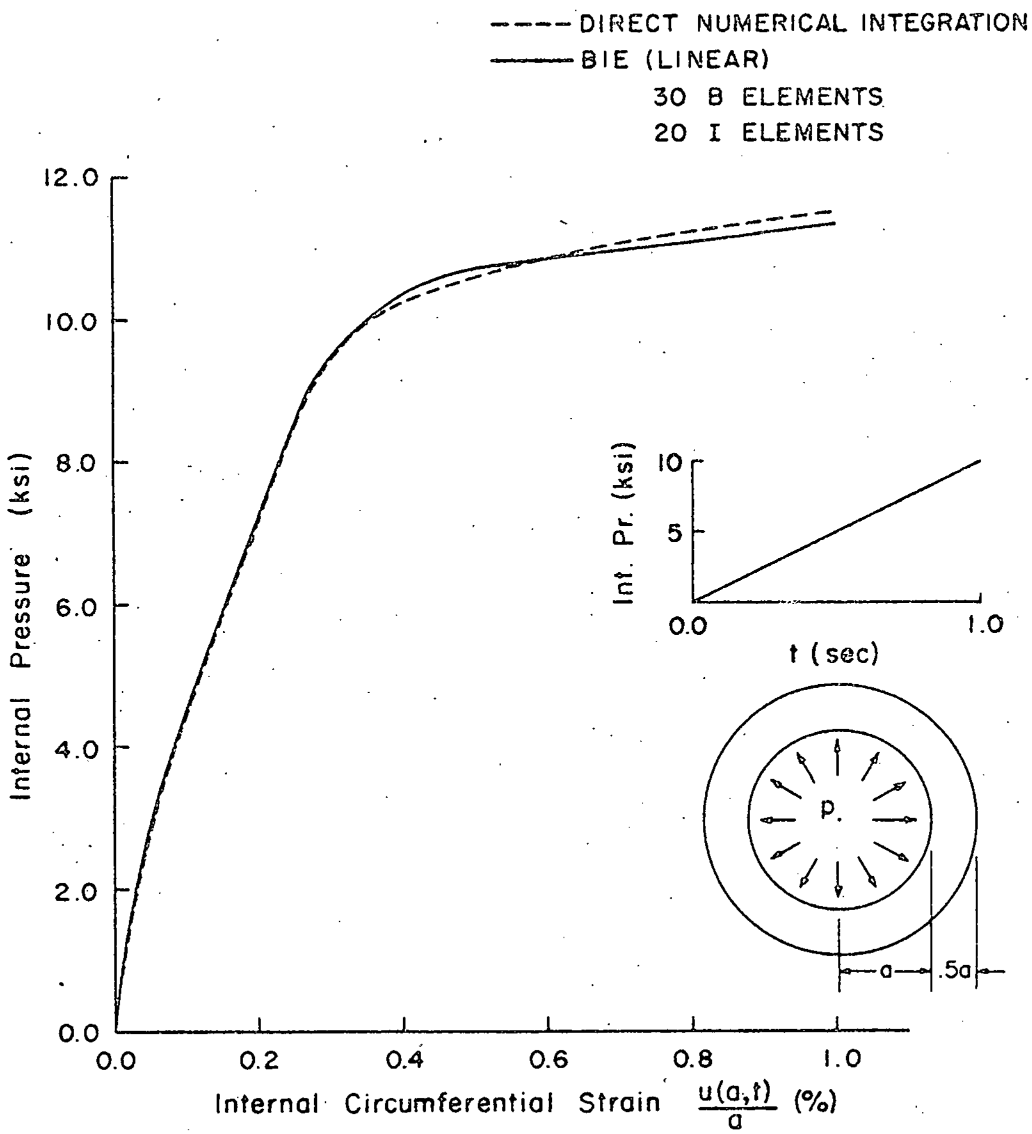

Figure 5. Comparison of direct and BIE solutions for circular plate with concentric circular cutout under internal pressure increasing at a constant rate. 304 SS at 200°C.

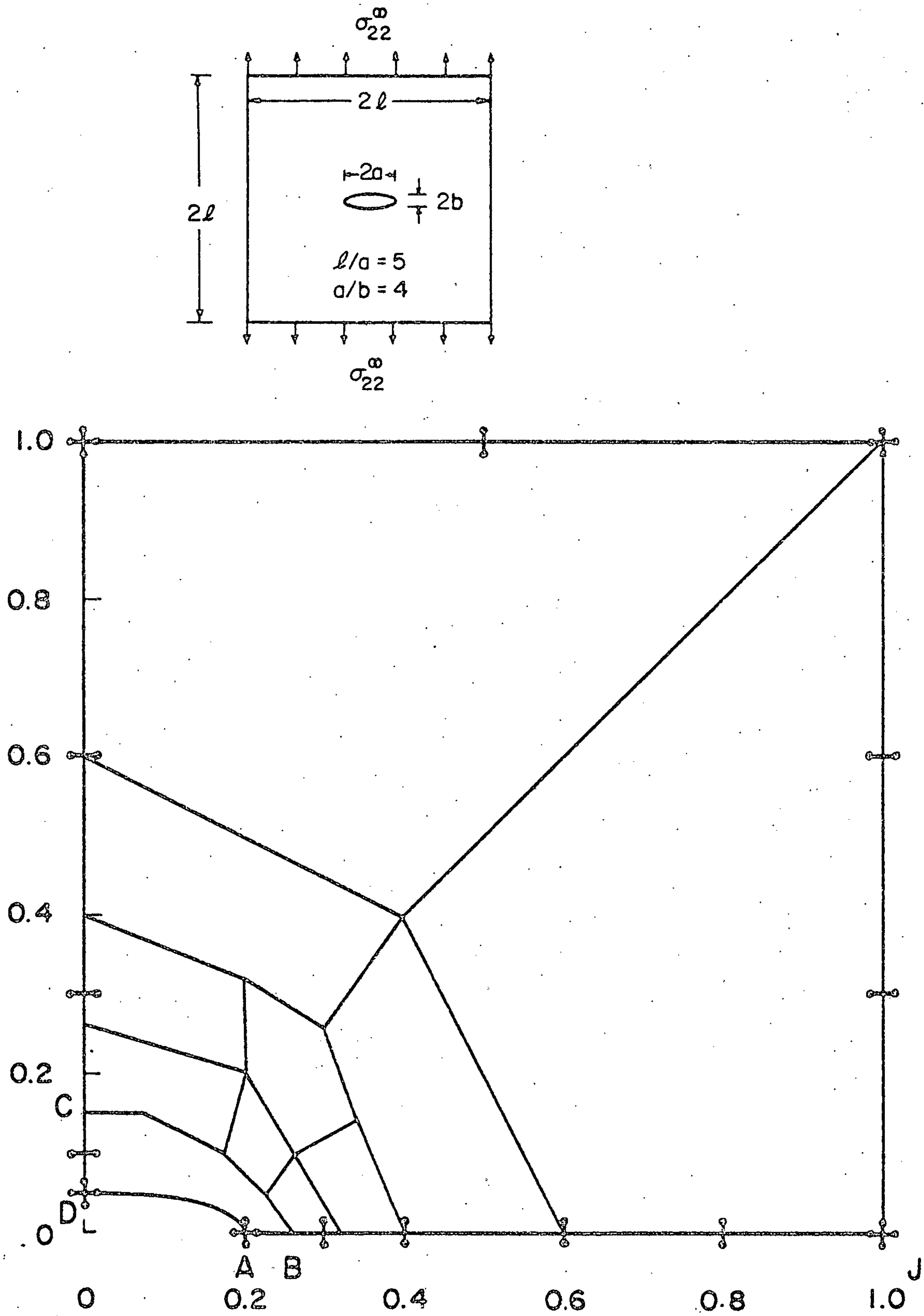

Figure 6(a). Boundary and internal elements for plate with elliptic cutout under uniaxial loading. 38 boundary elements and 30 internal elements.

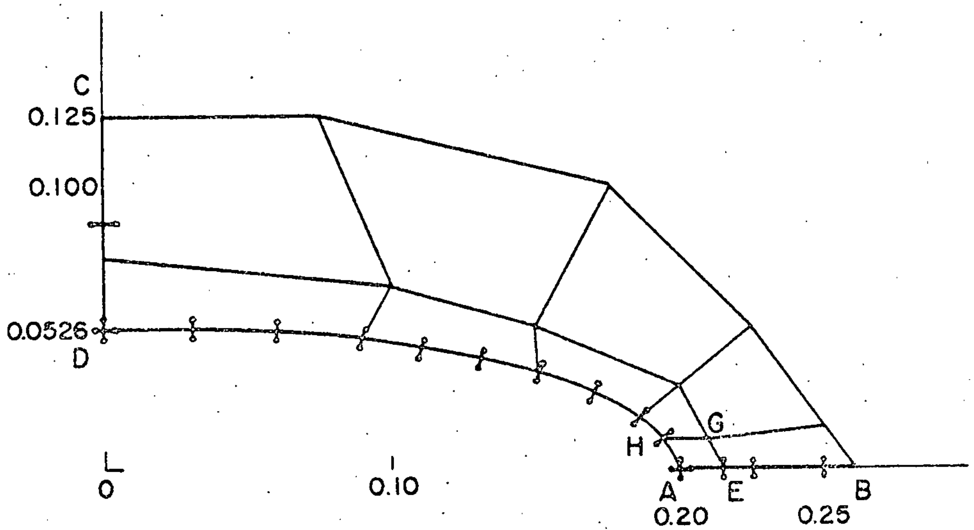

Figure 6(b). Further details of Figure 6(a).

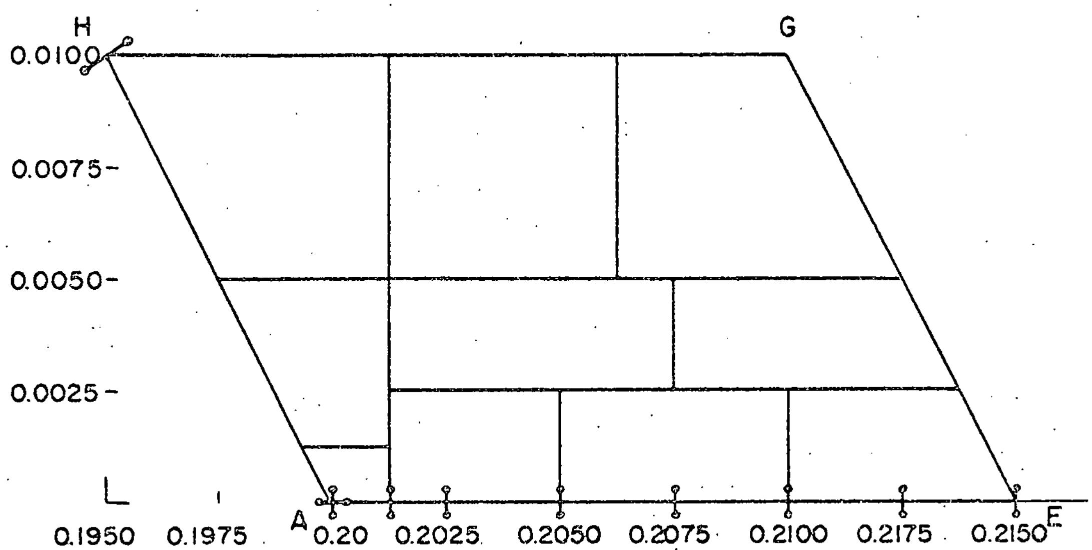

Figure 6(c). Further details of Figure 6(a).

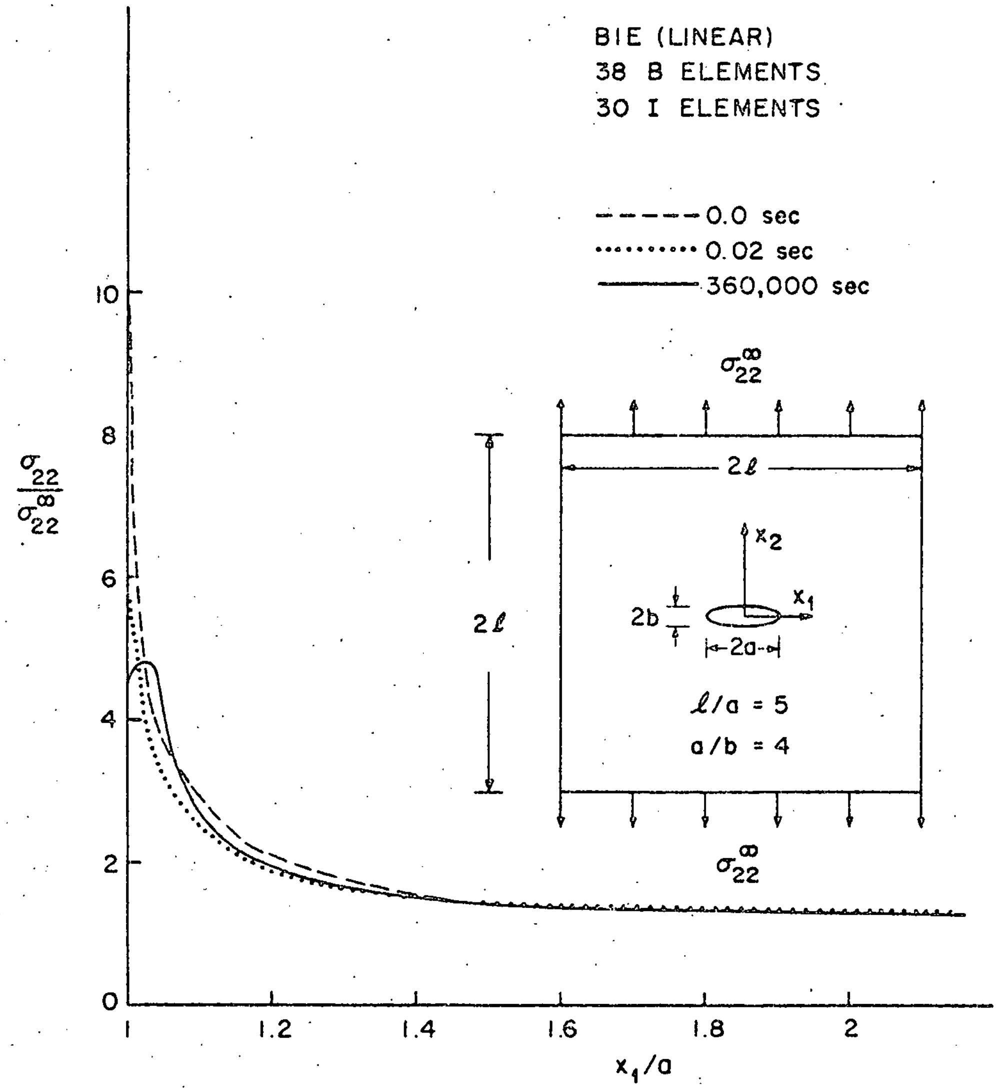

Figure 7. Stress redistribution on line AJ of Fig. 6(a) in an annealed 304 SS square plate with elliptic cutout under uniaxial tension at 400°C. $\sigma_{22}^{\infty} = 4$ ksi.